SUPPLEMENTARY MATERIAL

A. Equations solved for flow field calculation

Below are the equations used in the FORTRAN 77 computational fluid dynamics code used for determining the flow and other scalar fields in the thermodenuder. The equations are resented below in a similar manner as in Nenes et al. (2001).

$$\frac{\partial}{\partial t}(r\rho\phi) + \frac{\partial}{\partial z}(r\rho u\phi) + \frac{\partial}{\partial r}(r\rho v\phi) - \frac{\partial}{\partial z}\left(r\Gamma_\phi \frac{\partial \phi}{\partial z}\right) - \frac{\partial}{\partial r}\left(r\Gamma_\phi \frac{\partial \phi}{\partial r}\right) = S_\phi \quad \text{(A1)}$$

where the terms are substituted according to Table 3 for the various conserved quantities.

Table A1. Definition of source terms and transport coefficients for Equation (A1)

Conserved Quantity	ϕ	Γ_ϕ	S_ϕ
Continuity	1	0	0
z – momentum	u	μ	$-r\frac{\partial P}{\partial r} + r\frac{\partial}{\partial z}\left(\mu\frac{\partial u}{\partial r}\right) + \frac{\partial}{\partial r}\left(r\mu\frac{\partial v}{\partial r}\right) + J_{buoy}$
r – momentum	v	μ	$-r\frac{\partial P}{\partial r} + r\frac{\partial}{\partial z}\left(\mu\frac{\partial u}{\partial r}\right) + \frac{\partial}{\partial r}\left(r\mu\frac{\partial v}{\partial r}\right) - \frac{\mu v}{r}$
Heat	T	$\frac{k_a}{c_p}$	$\frac{\Delta H}{c_p}J_{volat}$
Organic Vapor	m_{evap}	ρD_{AB}	$-\rho J_{volat}$

The source term for thermal buoyancy effects is defined as

$$J_{buoy} = -\rho g_{\lambda_2}\left[\frac{T - T_{bulk}(r)}{T_{bulk}(r)}\right] \quad \text{(A2)}$$

where g_{λ_2} is the component of gravity in the r direction and $T_{bulk}(r)$ is the average temperature along z at position r.

The source (or sink) term for organic vapor is defined as

$$J_{volat} = \frac{\pi\rho}{2M}\sum_{i=1}^{n} N_i d_{pi}^2 \frac{dd_{pi}}{dt} \quad \text{(A3)}$$

where n is the number of size bins in the aerosol distribution with particular diameter and number concentration, and the rate of change is obtained from Equation (2), the aerosol evaporation equation.

B. Estimation of Uncertainty Ranges within the Optimization Algorithm

The Levenberg-Marquardt algorithm is an unconstrained optimization method which necessitated the use of a transformation for $\vec{x}^N$ to avoid it returning unphysical (i.e. negative) optimal values. In this study, the optimal physical volatility parameters ($\vec{x}^N$) are related to the optimal values obtained by ZXSSQ ($\vec{P}^N$) as $x_i = (P_i)^2$. To facilitate the optimization, ΔH was made to be the same magnitude as the saturation vapor pressure within the optimization space using the initial guesses of both parameters to obtain a scaling factor:

$$P^o(T_o) = (P_1)^2;\ \Delta H = \frac{(P_2)^2}{s} \tag{B1}$$

with $s = \frac{P^o_{initial}}{\Delta H_{initial}}$ and P_1, P_2 the optimal parameters determined by ZXSSQ. This variable transformation is taken into consideration in the uncertainty analysis.

ZXSSQ calculates the finite-difference Jacobian matrix ($\underline{J}$) through execution of the aerosol module at different settings of the optimization-space parameters, $\vec{P}^N$, during the minimization of the cost function. Each element of $\underline{J}$ is defined as the partial derivative of the residual terms with respect to perturbations in each parameter in the optimization space:

$$J_{ij} = \frac{\partial}{\partial P_j}\left(d_{p,out,i} - d_{pm,i}\right) = \frac{\partial d_{p,out,i}}{\partial P_j} - \frac{\partial d_{pm,i}}{\partial P_j} \cong \frac{\Delta d_{p,out,i}}{\Delta P_j} - \frac{\Delta d_{pm,i}}{\Delta P_j} \tag{B2}$$

During the parameter optimization, $\Delta d_{p,out,i} = 0$ since $d_{p,out}$ is unaffected by changes in P_j; thus $\underline{J}_{ij}$ can be interpreted as the $d_{pm,i}$ sensitivity to variations in P_j (with a sign change). The volatility parameter uncertainty ranges are determined by first applying $\underline{J}$ to calculate ΔP_{ij} for a given variation in inlet diameter, $\Delta d_{p,out,i}$, which is taken to represent the uncertainty in the measured outlet diameters (i.e., the width of the DMA transfer function). In this case, $\Delta d_{pm,i} = 0$ and the relationship to $\underline{J}$ is defined as

$$\Delta P_{ij} = \frac{\Delta d_{p,out,i}}{J_{ij}} \tag{B3}$$

Propagating the relative uncertainty in P_j through to x_j we get

$$\frac{\Delta x_{ij}}{x_j} = 2\left(\frac{\Delta P_{ij}}{P_j}\right) = \frac{2\Delta d_{p,out,i}}{P_j J_{ij}} \tag{B4}$$

This provides an estimate of the uncertainty in each parameter, x_j, at every observed outlet diameter, $d_{p,out}$. These estimates of uncertainty in the same parameter do not have much meaning when expressed individually, as all observations were combined in the model fitting. They may also vary considerably from measurements to measurement. Therefore, a weighted average of the uncertainty across all measurements is taken as

$$\Delta x_j = \frac{\sum_i^M w_i \Delta x_{ij}}{\sum_i^M w_i} \tag{B5}$$

with weights, w_i, defined as the observed diameter change experienced by the aerosol $w_i = \left(d_{p,in,i} - d_{p,out,i}\right)$.

C. Modal diameters for non-volatile residuals and multiply-charged particles

To confirm that the smallest mode is consistent with the amount of impurities in the aerosol, the non-volatile residual diameter, $d_{p,resid}$, was estimated from the reported fractional mass purity (f) for each compound considered, the inlet diameter, $d_{p,in}$, the density of the organic compound (ρ_{org}), and an assumption about the density of the residual matter (ρ_{resid}):

$$d_{p,resid} = \left(d_{p,in}^3 \frac{\rho}{\rho_{resid}} (1 - f) \right)^{1/3} \quad \text{(C1)}$$

$d_{p,resid}$ is computed twice, assuming ρ_{resid} is equal to the density of NaCl (ρ_{NaCl}) and assuming it has the same density as the organic component (ρ_{org}). The two calculations were performed to illustrate the uncertainty associated with the residual diameter. The uncertainty in the inlet diameter measurement (from the width of the DMA transfer function) is also propagated through the estimate of the residual diameter. These calculated values were compared with the $d_{p,out}$ values of the lowest diameter mode from the SMPS data. Figure S3 illustrates the comparison for each organic acid at the reported mass purities. The data appear to fall into two distinct sets of points in the figures: one close to the 1:1 line and another well underneath it. For malonic acid, the mass purity was assumed to be 98%. Particular observations were considered to be affected by low-volatility material when values of $d_{p,out}$ and $d_{p,resid}$ fall within uncertainty near the 1:1 line. Data that was just outside of agreement were also considered to be contaminated. The contribution of impurities from the deionized water is not thought to be important, as atomization of pure deionized water did not show any appreciable particle concentrations (not shown).

The electrical mobility of particles in the DMA is related to particle properties by

$$Z_e = \frac{q C_c}{3\pi\mu d_p} \quad \text{(C2)}$$

with μ defined as the viscosity of air, q is the number of elementary charges on the particle, and $C_c(d_p) = 1 + \frac{2\lambda}{D_p}\left[1.257 + 0.4\exp\left(-\frac{1.1 d_p}{2\lambda}\right)\right]$ is the Cunningham slip correction factor (Seinfeld and Pandis, 2006). The presence of double-charged particles can explain the largest diameter mode in the occasional tri-modal distribution observed for thermodenuded aerosol, and is determined as follows. Considering a spherical aerosol with the same electrical mobility as the single-charged aerosol with $d_{p,in}$, the double-charged diameter, $d_{p,2x}$, application of Equation (S2) yields

$$d_{p,2x} = \frac{2C_c(d_{p,2x})}{1C_c(d_{p,in})} d_{p,in} \quad \text{(C3)}$$

The dependence of C_c on particle diameter requires the calculation to be iterated until it converges to a particular value of $d_{p,2x}$. These $d_{p,2x}$ were then used to initialize the aerosol module using the same volatility parameters estimated from the fitting of the middle mode of the thermodenuded particles. The model results (d_{pm}) were compared against the largest diameter mode in the observed size distribution ($d_{p,out}$) (Figure S4). Suberic and pimelic acid results are not shown because neither was observed to exhibit trimodal size distributions in the measurements, likely because the former did not volatilize enough while the latter was too volatile. Figure S4 clearly shows that the model-predicted outlet diameter for the double-charged particles agrees with the largest diameter mode, regardless of the number of modes observed; thus, the third (rightmost on SMPS scan) mode was not observed when the outlet diameters for the double-charged and single-charged outlet diameters were similar. This explanation is

consistent with the laboratory setup where the particle charge distribution was re-equilibrated at the second DMA downstream of the thermodenuder.

The additional possibility that nucleation in the thermodenuder cooling section could cause the smallest size mode to appear in the SMPS scans is considered. Direct comparison of the SMPS and CPC measured total particle concentrations before and after the thermodenuder is inconclusive, considering the problems associated with the SMPS inversion process when the sample aerosol are charge neutralized a second time before the second DMA. Thus, an alternative approach is considered to determine if nucleation could consistently explain the appearance of the smallest mode. For this, we estimate the maximum saturation ratio, Rn, of the gas phase as follows. To first order, the organic vapor pressure at any point in the thermodenuder is equal to the vapor that initially enters it plus the amount that volatilizes from the aerosol phase

$$P_\infty = P_\infty(z=0) + \frac{m_{evap} R T_\infty}{M} \quad \text{(C4)}$$

where m_{evap} is the volatilized mass concentration (kg m^{-3} air), R is the ideal gas constant, and T_∞ is the local temperature. Since aerosols in this study are generated by atomization and subsequent rapid drying of aqueous solution, little time is allowed for equilibration between the aerosol and vapor phases, so we assume that P_∞(z = 0) is negligible. We then express $R_n = \frac{P_\infty}{P^o}$, as

$$R_n = \frac{P_\infty(z=0)}{P^o} + \frac{m_{evap} R T_\infty}{M P^o} \cong \frac{m_{evap} R T_\infty}{M P^o} \quad \text{(C5)}$$

The maximum saturation ratio is calculated at the expected temperature of the cooling section, 25^{o}C, using literature values for the saturation vapor pressures (Figure S5). Of particular interest are the results for malonic (S5d) and suberic (S5e) acids. Based on this calculation, it would be much more likely for nucleation to occur in the suberic acid experiments than in the malonic acid experiments because the saturation ratios at the highest temperatures for the former could be up to over twelve times higher than the latter – which were, moreover, subsaturated. However, visual inspection of the separate SMPS scans for all of the malonic and suberic acid results shows that the appearance of the smallest mode occurs more often (most scans) for malonic acid but inconsistently for suberic acid (S6). Thus, the hypothesis that vapor buildup could be causing nucleation in the cooling section appears to be inconsistent with the data. Considering that a more consistent alternative hypothesis exists (above), the smallest diameter modes in the SMPS are more likely do to residual non-volatile cores that arising from nucleation in the thermodenuder.

Data tables for each set of experiments are presented in the following section. Errors in the size distribution measurement could influence the optimization; this is particularly important when packaged SMPS analysis software, such as the Aerosol Instrument Manager (AIM) program (TSI, version 8.1.0.0), is used as it automatically outputs the mode with the highest concentration, even if it may not represent the mode that expresses the true particle volatility. For this reason we present modal diameters automatically identified by AIM and that using our method that corrects for the presence of doublets and non-volatile cores. Comments indicate points omitted due to non-volatile core interference (NV) and points adjusted to an alternative mode considering either non-volatile core interference and presence of double-charged particles or both (AM).

D. Data Inversion Sensitivity Tests

Volatility parameter retrievals were repeated for various assumptions regarding certain aspects of the model. First, the parameters retrieved for all experimental simulations were repeated for the case where just the heating section was considered and are compared to simulations that included the full model geometry (Figure S7a). Including only the heating section results in an increase of the retrieved saturation vapor pressures by about a factor of two on average with a corresponding slight decrease in the enthalpy change. This is associated with the comparably shorter residence time in the model domain in that case which then requires a higher volatility across all temperature settings in order to fit the experimental data.

Second, the parameter retrieval for all simulations was repeated for two different cases of different accommodation coefficients: 0.1 and 0.01, compared to the base case of unity (Figure S7b). The results indicate that, in general, a decrease in accommodation coefficient by an order of magnitude results in a corresponding increase in saturation vapor pressure. This is the greatest sensitivity observed for our experimental conditions but is actually dampened by an increase in the aerosol mass concentration (not shown).

Additional sensitivity tests are also presented to assess the sensitivity of the parameter retrieval to experimental variation in relevant temperatures. These tests were done for one of the organic compounds under consideration (adipic acid) under both the assumption of unity accommodation coefficient and using the available literature value (the two separate points in Figure S7c, d). The experimental conditions for the adipic acid measurements are less than+/- 1 K in the thermodenuder setpoint temperature at the first thermocouple (wall boundary condition) and +/- 5 K in the thermodenuder inlet temperature. The wall temperature variation has a larger potential impact than variations in the inlet temperature; however, the variation is still small and within the estimated uncertainty range.

E. Table of literature values

Table E1. Compiled literature values for reference volatility parameters. The listed values regard either vaporization or sublimation as indicated by the phase designation – either solid (S) or supercooled liquid (L). If the source did not provide adequate information to make such a conclusion, then "?" is used to indicate that phase is not specified. Uncertainties presented in the literature source are translated (if necessary) to maximum and minimum bounds with an average value. *C** is calculated as in Table 3.

	P^o(298K) ($Pa \times 10^{-5}$)			ΔH ($J\ mol^{-1} \times 10^5$)			Phase	C^*(298K) ($\mu g\ m^{-3}$)
	Avg.	Max.	Min.	Avg.	Max.	Min.		
Adipic Acid								
Bilde et al. (2003)	0.98	1.47	0.49	1.54	1.60	1.48	S	0.578
Saleh et al. (2010) [a]	3.30	4.20	2.40	1.32	1.40	1.24	S	1.947
Saleh et al. (2010) [h]	4.20	6.40	2.00	1.26	1.47	1.05	S	2.477
Salo et al. (2010)	5.80	7.60	4.40	0.97	1.05	0.89	S	3.421
Cappa et al. (2007)	0.26	0.36	0.16	1.45	1.50	1.40	S	0.153
Riipinen et al. (2007)	0.40	0.50	0.30	1.48*	1.70*	1.26*	S	0.236
Riipinen et al. (2007)	17.00	20.00	14.00	1.13	1.35	0.91	L	10.03
Chatto. et al. (2001)	1.70	-	-	1.40	-	-	?	1.003
Saleh et al. (2009)	3.40	4.60	2.00	1.35	1.48	1.22	S	2.005
Booth et al. (2009)	0.33	0.71	-0.06	1.19	1.45	0.93	S	0.193
Booth et al. (2010)	21.40	37.45	5.35	0.83	1.09	0.57	L	12.62
Azelaic Acid								
Bilde et al. (2003)	0.60	0.90	0.30	1.53	1.77	1.29	S	0.456
Saleh et al. (2010) [a]	1.40	1.90	0.90	1.45	1.60	1.30	S	1.064
Saleh et al. (2010) [h]	0.90	1.20	0.60	1.58	1.75	1.41	S	0.684
Salo et al. (2010)	4.70	5.50	4.00	0.96	1.01	0.91	S	3.571
Cappa et al. (2007)	1.00E-03	1.60E-03	4.00E-04	1.78	1.83	1.73	S	7.6E-04
Malonic Acid								
Bilde et al. (2003)	36.00	54.00	18.00	0.92	1.07	0.77	S	15.12
Soonsin et al. (2010)	43.00	58.00	28.00	0.96	1.07	0.85	L	18.06
Soonsin et al. (2010)	8.00	10.90	5.10	1.07	1.11	1.03	S	3.360
Riipinen et al. (2007)	5.20	6.30	4.10	1.41*	1.66*	1.16*	S	2.184
Riipinen et al. (2007)	49.00	59.00	39.00	1.22	1.47	0.97	L	20.58
Booth et al. (2009)	57.30	68.70	45.90	0.92	0.96	0.88	S	24.07
Booth et al. (2010)	319.00	558.25	79.75	0.73	0.77	0.69	L	134.0
Pope et al. (2010)	67.00	93.00	55.00	1.42	1.62	1.22	L	28.14
Succinic Acid								
Bilde et al. (2003)	3.90	5.85	1.95	1.38	1.49	1.27	S	1.859

Salo et al. (2010)	6.40	8.40	4.60	1.12	1.24	1.00	S	3.050
Cappa et al. (2007)	3.20	3.80	2.60	1.28	1.30	1.26	S	1.525
Riipinen et al. (2007)	2.50	3.10	1.90	1.37[*]	1.60[*]	1.14[*]	S	1.192
Riipinen et al. (2007)	99.00	123.00	75.00	1.04	1.27	0.81	L	47.19
Soonsin et al. (2010)	170.00	220.00	120.00	1.06	1.14	0.98	L	81.03
Soonsin et al. (2010)	0.60	0.81	0.39	1.25	1.33	1.17	S	0.286
Saleh et al. (2009)	37.00	48.00	26.00	0.88	0.91	0.85	S	17.64
Booth et al. (2009)	11.30	16.00	6.60	0.93	0.99	0.87	S	5.386
Booth et al. (2010)	386.00	675.50	96.50	0.62	0.68	0.56	L	184.0
Suberic Acid								
Bilde et al. (2003)	0.12	0.18	0.06	1.84	1.96	1.72	S	0.084
Chatto. et al. (2001)	0.34	-	-	1.48	-	-	?	0.239
Salo et al. (2010)	1.40	2.00	1.00	1.01	1.11	0.91	S	0.984
Cappa et al. (2007)	0.02	0.03	0.01	1.68	1.75	1.61	S	0.013
Booth et al. (2011)	2.23	3.90	0.56	1.53[†]	1.65[†]	1.41[†]	L	1.568
Pimelic Acid								
Bilde et al. (2003)	5.10	7.65	2.55	1.47	1.58	1.36	S	3.297
Chatto. et al. (2001)	1.20	-	-	1.78	-	-	?	0.776
Salo et al. (2010)	17.00	25.00	12.00	1.27	1.47	1.07	S	10.99
Cappa et al. (2007)	0.39	0.45	0.33	1.53	1.57	1.49	S	0.252
Booth et al. (2011)	26.30	46.03	6.58	1.23[†]	1.34[†]	1.12[†]	L	17.00
Saleh et al. (2009)	7.20	8.90	5.50	1.49	1.59	1.39	S	4.655

[a]Atomization used as the aerosol generation technique
[h]Homogeneous nucleation used as the aerosol generation technique
[*]ΔH_{sub} calculated by using equation and reference values for ΔH_{fus} (Yaws, 2003; Booth et al., 2010) and heat capacity from liquid results
[†]ΔH_{vap} obtained from Bilde et al. (2003) estimates of solid values

F. Mode diameter data tables from experiments

Table F1. Adipic acid average mode diameter data

Set point temperature (^{o}C)	$d_{p,in}$ (nm)	$d_{p,out}$ observed by AIM (nm)	$d_{p,out}$ using correct mode (nm)	Comment
40	66.0	61.5	61.5	
	88.3	85.1	85.1	
	111	106	106	
	133	129	129	
	155	151	151	
50	65.9	49.0	49.0	
	88.2	72.8	72.8	
	110	94.7	94.7	
	1.33	118	118	
	1.55	141	141	
60	65.8	17.5	-	NV
	88.2	22.5	-	NV
	110	28.9	57.3	AM
	132	59.8	82.1	AM
	154	107	107	

Table F2. Azelaic acid average mode diameter data

Set point temperature (^{o}C)	$d_{p,in}$ (nm)	$d_{p,out}$ observed by AIM (nm)	$d_{p,out}$ using correct mode (nm)	Comment
40	65.3	58.0	58.0	
	87.5	82.0	82.0	
	110	106	106	
	132	126	126	
	153	151	151	
50	65.3	19.1	35.9	AM
	87.5	60.8	60.8	
	110	88.2	88.2	
	132	113	113	
	153	136	136	
60	65.4	11.8	-	NV
	87.6	16.3	-	NV
	110	20.9	-	NV
	132	24.1	56.0	AM
	154	27.6	87.1	AM

Table F3. Malonic acid average mode diameter data

Set point temperature (^{o}C)	**$d_{p,in}$ (nm)**	**$d_{p,out}$ observed by AIM (nm)**	**$d_{p,out}$ using correct mode (nm)**	**Comment**
40	65.5	16.0	33.0	AM
	87.7	54.3	54.3	
	110	81.1	81.1	
	132	104	104	
	154	129	129	
50	65.5	25.9	-	NV
	87.7	30.3	-	NV
	110	34.6	-	NV
	132	35.2	-	NV
	154	39.2	52.7	AM
60	65.5	25.9	-	NV
	87.7	30.0	-	NV
	110	34.0	-	NV
	132	34.2	-	NV
	154	38.5	-	NV

Table F4. Pimelic acid average mode diameter data

Set point temperature (^{o}C)	**$d_{p,in}$ (nm)**	**$d_{p,out}$ observed by AIM (nm)**	**$d_{p,out}$ using correct mode (nm)**	**Comment**
40	65.9	17.7	-	NV
	88.2	30.9	46.7	AM
	110	74.6	74.6	
	133	98.2	98.2	
	155	125	125	
50	65.8	16.8	-	NV
	88.1	21.7	-	NV
	110	26.9	-	NV
	132	31.4	-	NV
	154	36.3	-	NV
60	65.9	16.8	-	NV
	88.2	21.7	-	NV
	110	26.9	-	NV
	132	31.8	-	NV
	155	35.9	-	NV

Remarks: Do not expect to obtain a robust parameter fit due to non-volatile core interference.

Table F5. Suberic acid average mode diameter data

Set point temperature (^{o}C)	**$d_{p,in}$ (nm)**	**$d_{p,out}$ observed by AIM (nm)**	**$d_{p,out}$ using correct mode (nm)**	**Comment**
40	65.9	66.1	65.9	Growth (w/in uncert.)
	88.4	88.2	88.2	
	111	109	109	
	133	131	131	
	155	157	155	Growth (w/in uncert.)
50	66.1	61.5	61.5	
	88.5	85.1	85.1	
	111	109	109	
	133	131	131	
	155	151	151	
60	66.1	18.7	40.9	AM
	88.5	68.6	68.6	
	111	95.9	95.9	
	133	120	120	
	155	144	144	

Table F6. Succinic acid average mode diameter data

Set point temperature (^{o}C)	$d_{p,in}$ (nm)	$d_{p,out}$ observed by AIM (nm)	$d_{p,out}$ using correct mode (nm)	Comment
40	65.7	52.3	52.3	
	88.0	76.4	76.4	
	110	98.2	98.2	
	132	122	122	
	154	146	146	
50	65.7	22.5	-	NV
	88.0	29.4	52.7	AM
	110	79.1	79.1	
	132	102	102	
	154	126	126	
60	64.5	15.1	-	NV
	86.7	19.9	-	NV
	109	24.1	-	NV
	131	28.9	-	NV
	154	34.6	-	NV

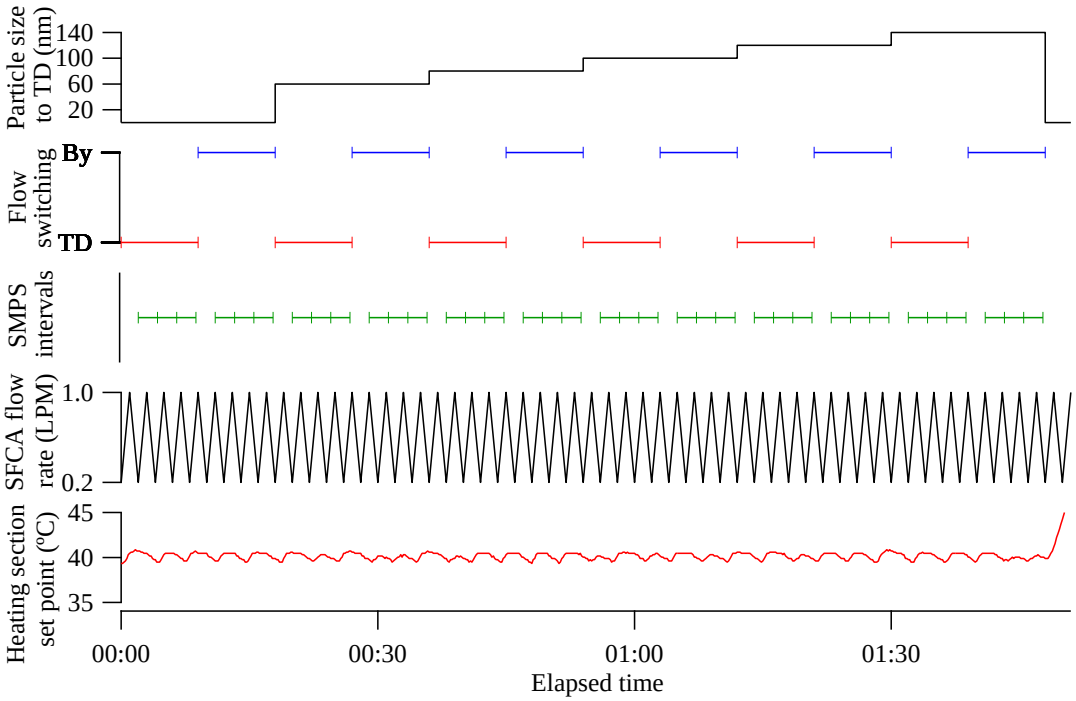

Figure S1. Sampling schedule for bypass (By) and thermodenuder (TD) aerosol samples during a single heating section set point temperature.

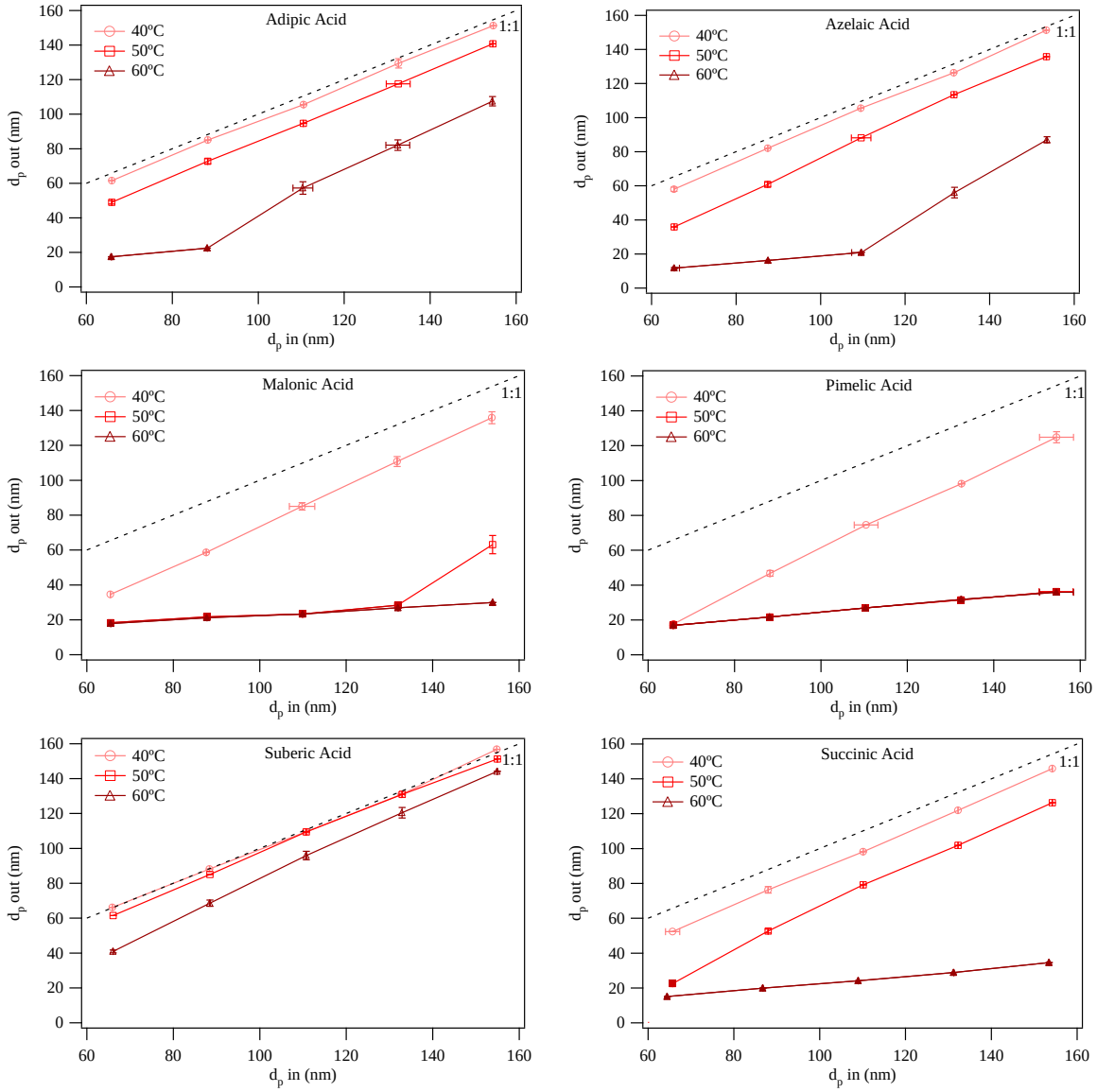

Figure S2. Change in diameter for several pure organic acids after passing through the thermodenuder at 40, 50, and 60°C. Solid symbols represent points resulting from non-volatile cores and discarded from model fitting. Vertical and horizontal error bars represent the standard deviation in the mode measured during three SMPS scans collected from the thermodenuder and bypass, respectively.

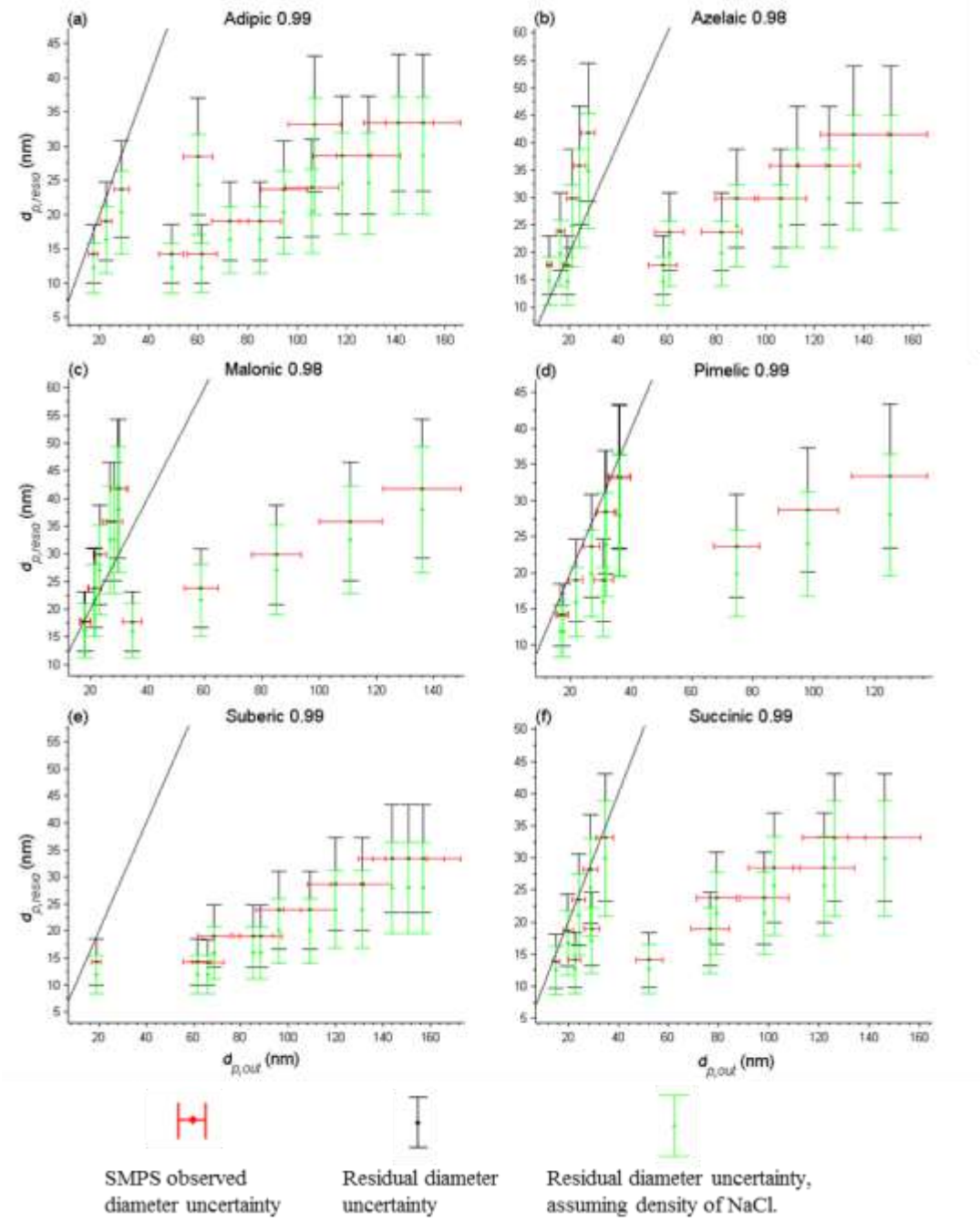

Figure S3. Observed outlet diameter against the expected residual diameter calculated by Equation (S1). The uncertainty in the observations is based on the DMA transfer function for a 10:1 sheath to aerosol flow ratio. The uncertainty in the calculated residual diameters is propagated through Equation (S1). Uncertainty in the residual component density is represented by choosing two possible densities: NaCl or the organic compound (black/green).

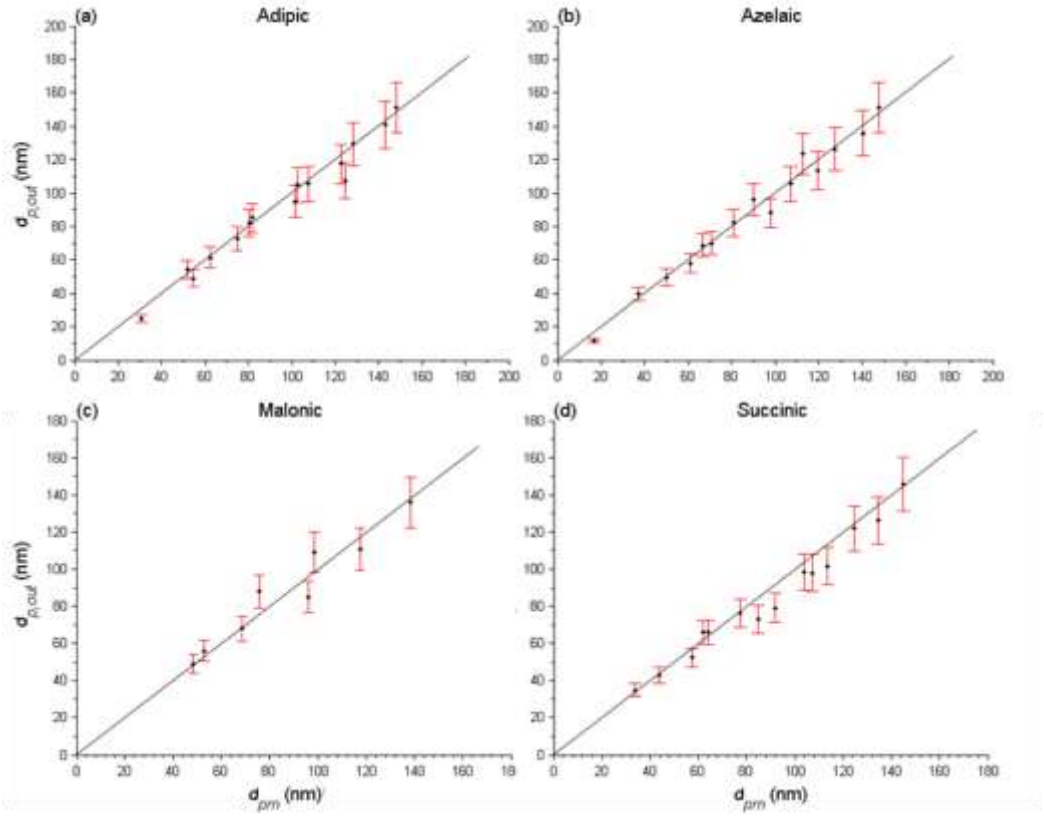

Figure S4. Output of the thermodenuder model (d_{pm}) when it was initialized with the calculated double-charged diameters ($d_{p,2x}$) versus the largest observed outlet mode diameter ($d_{p,out}$). Error bars represent the measurement uncertainty from the DMA transfer function.

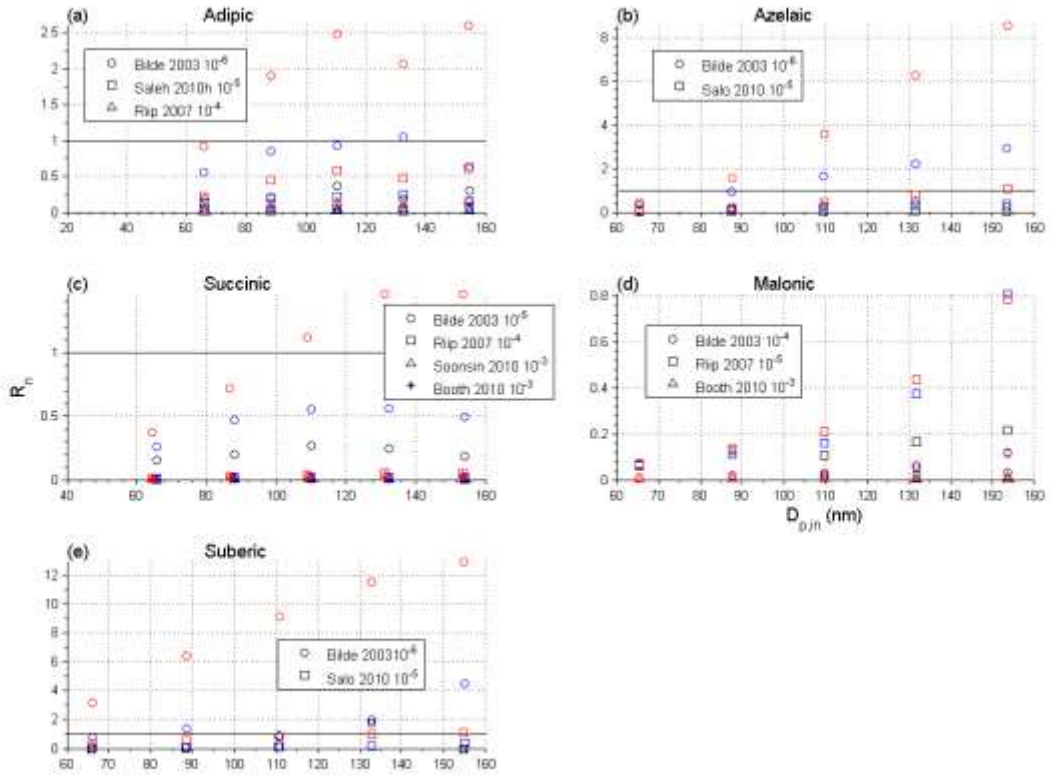

Figure S5. The value of R_n is compared against the inlet diameter ($d_{p,in}$) and is calculated for a variety of P^o indicated by the legend entries which reference corresponding rows in Table 3 of the main text and at a nominal cooling section temperature of 25°C. The color scheme used to indicate the temperature set point is the same as in Figure 7. In effect, R_n provides a maximum possible saturation ratio in the cooling section, based on thermodynamic parameters in the literature and the measured experimental data.

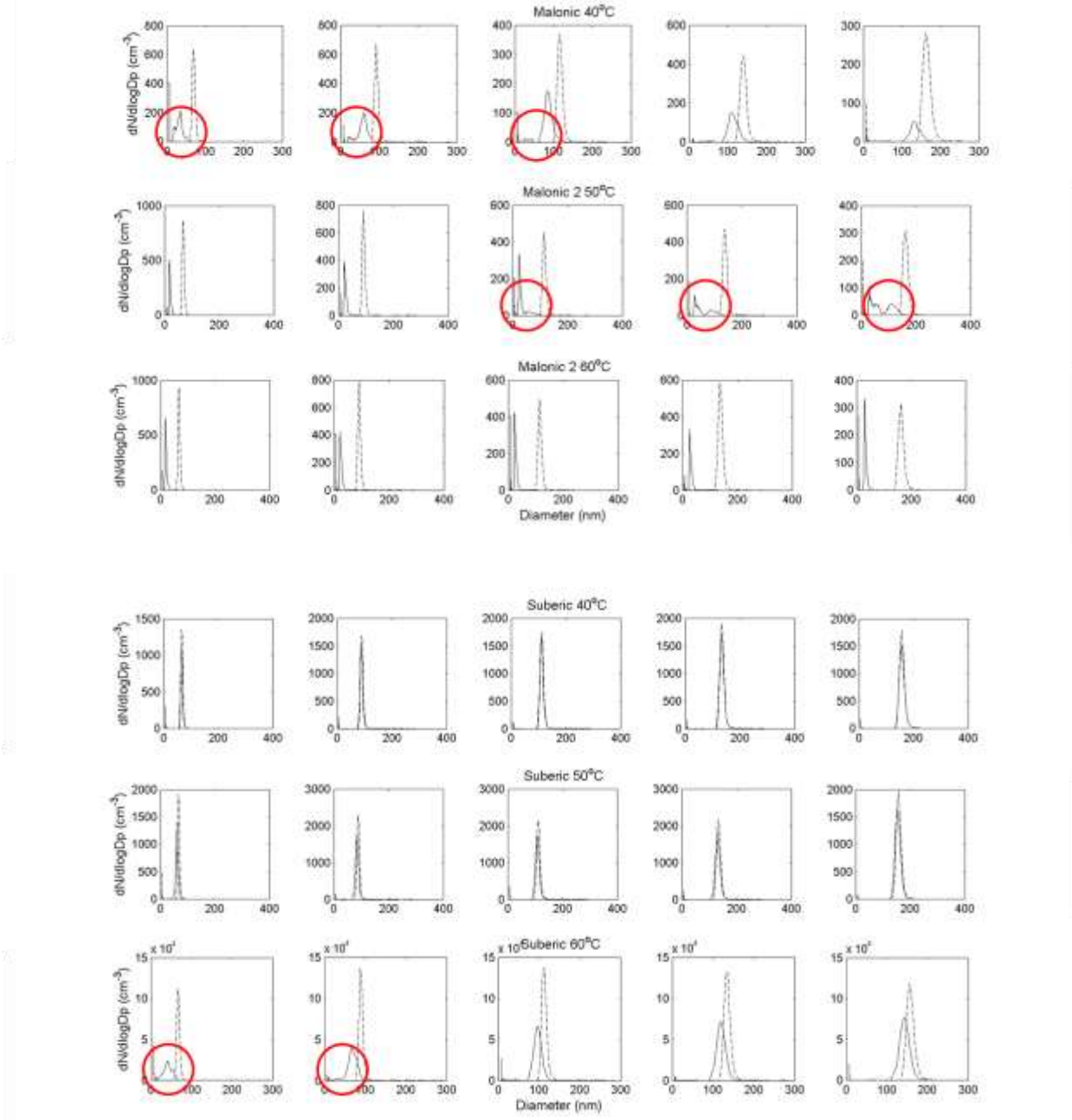

Figure S6. Sample scans of thermodenuded malonic (top 3 rows) and suberic acid aerosol at temperature set points of 40, 50, and 60°C

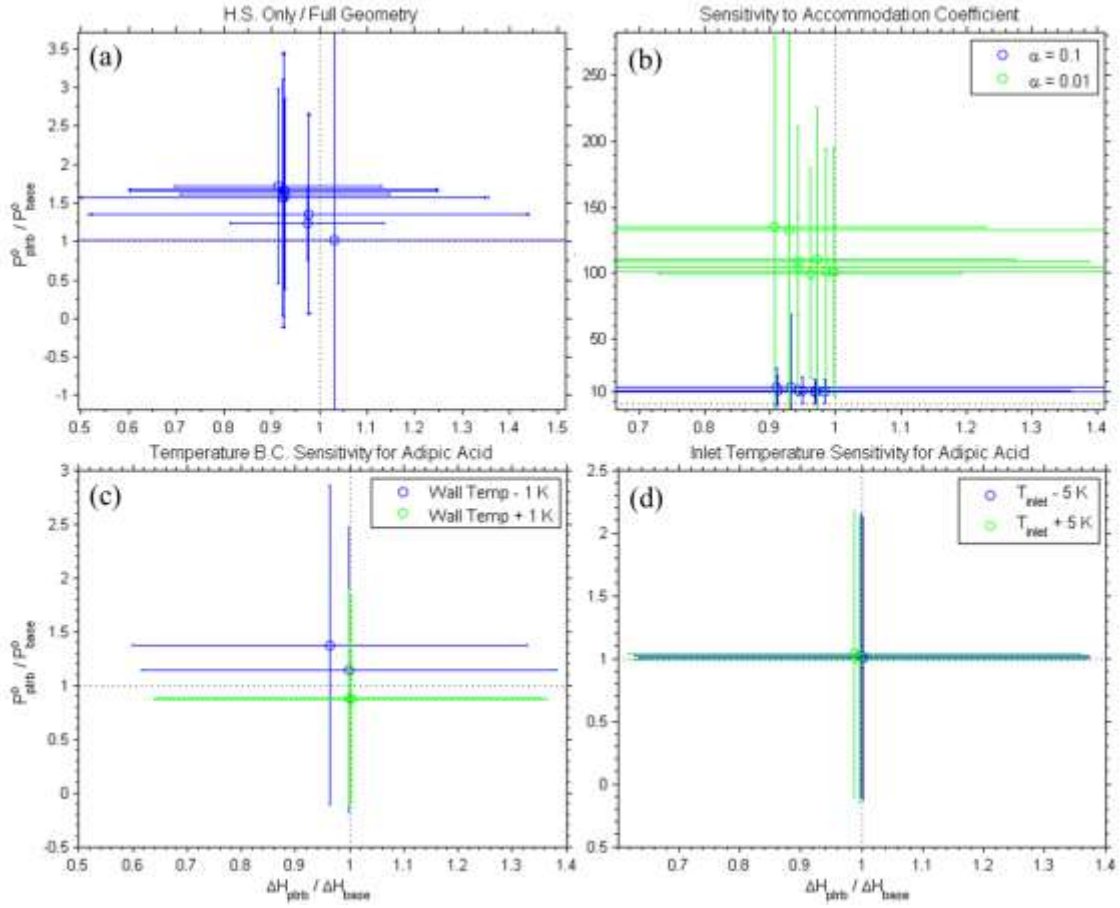

Figure S7. Model sensitivity tests for (a) whether or not the cooling section is considered, (b) variation in the accommodation coefficient, (c) variation in the wall temperature boundary conditions, and (d) variation in the inlet temperature.